Journal of Alloys and Compounds 504 (2010) 573–578

Contents lists available at ScienceDirect

Journal of Alloys and Compounds

journal homepage: www.elsevier.com/locate/jallcom

Energy transfer and 1.8 μm emission in Tm^{3+}/Yb^{3+} codoped lanthanum tungsten tellurite glasses

Kefeng Li[a,b,*], Qiang Zhang[a,b], Gongxun Bai[a,b], Sijun Fan[a,b], Junjie Zhang[a], Lili Hu[a]

[a] Key Laboratory of Materials for High Power Laser, Shanghai Institute of Optics and Fine Mechanics, Chinese Academy of Sciences, Shanghai 201800, PR China
[b] Graduate School of Chinese Academy of Sciences, Beijing 100039, PR China

ARTICLE INFO

Article history:
Received 29 March 2010
Received in revised form 26 May 2010
Accepted 29 May 2010
Available online 11 June 2010

Keywords:
Tungsten tellurite glass
Tm^{3+}/Yb^{3+} codoping
1.8 μm emission
Judd–Ofelt theory

ABSTRACT

Tm^{3+}/Yb^{3+}-codoped lanthanum tungsten tellurite (TWL) glasses are prepared by melt-quenching method and the thermal stability of the glasses is analyzed. To evaluate the spectroscopic properties of Tm^{3+} in TWL glass, the Judd–Ofelt intensity parameters (Ω_t $t = 2, 4, 6$), radiative transition rates, radiative lifetimes, and branching ratios of Tm^{3+} are calculated based on the absorption spectrum. The 1.8 μm emission of the samples are investigated under the excitation of 980 nm LD. Large product of emission cross-section and lifetime ($\sigma_{em}\tau_R$) of Tm^{3+}: $^3F_4 \rightarrow {}^3H_6$ is obtained, and the maximum gain coefficient at around 1835 nm is 3.6 cm^{-1}. The energy transfer processes of Yb^{3+}–Yb^{3+} and Yb^{3+}–Tm^{3+} are analyzed, the results show that the Yb^{3+} ions can transfer their energy to Tm^{3+} ions with a large energy transfer coefficient, and a maximum efficiency of 89%.

1. Introduction

In recent years, solid state lasers operating in the ~2 μm region have a growing interest for their applications in biomedical, military, remoting sensing, and eye-safe lidar [1]. Tm^{3+} doped materials with $^3F_4 \rightarrow {}^3H_6$ transition are appropriate systems for generating such laser emission. The $^3F_4$ level of Tm^{3+} can be populated using sensitizer ions such as Yb^{3+} and Er^{3+} [2–4]. In particular, Tm^{3+} doped glasses sensitized by Yb^{3+} are recognized as efficient systems for obtaining strong luminescence in both the infrared and visible range of the spectrum [4,5]. This is due to the large absorption and emission cross-section, relatively long lifetime, and simply energy level scheme of Yb^{3+}. Moreover, Yb^{3+} can be efficiently pumped by a laser diode (LD) near 970 nm which is one of the most popular and convenient commercial pump sources [6]. Indeed, an efficient ~2 μm laser with power scaling up to 75 W has already been developed in Tm/Yb codoped silica fiber pumped by a 975-nm LD [7]. Yb^{3+} can transfer its energy to Tm^{3+} via a nonresonant energy tansfer processes assisted by one or more phonons [8]. Fast diffusion among the Yb^{3+} ions can enhance the efficiency of the nonresonant energy transfer from Yb^{3+} to Tm^{3+} by $^2F_{5/2} + {}^3H_6 \rightarrow {}^2F_{7/2} + {}^3H_5$ [5,9]. So, materials with a high solubility of Yb^{3+} are prefered. Materials with low phonon energy will enhance the upconversion luminescence, on the other hand, back transfer processes will be significant in a high phonon energy host, both characteristics have a negative contribution to the 1.8 μm emission [9,10]. It is therefore desirable to find host materials with intermediate phonon energy and large solubility of Tm^{3+} and Yb^{3+}, in which Yb^{3+} can efficiently transfer its energy to Tm^{3+}.

Lanthanum–Tungsten–Tellurite glasses are good candidates satisfying these demands. They express intermediate phonon energy (920 cm^{-1}) [11], which is intervenient between that of the fluoride glasses and silicate glasses, high refractive index (2.133), good thermal stability, low coefficient of thermal expansion, as well as large solubility of rare earth (RE) ions. In this paper, a Lanthanum–Tungsten–Tellurite glasses with molar composition $10La_2O_3$–$30WO_3$–$60TeO_2$ (TWL) is selected as a doping matrix, the Judd–Oflet parameters, spontaneous radiative transition probabilities, branching ratios and lifetimes of Tm^{3+} are calculated to evaluate the spectroscopic properties of Tm^{3+} in TWL glass. The 1.8 μm emission characteristic and energy transfer processes of Tm^{3+} and Yb^{3+} in TWL glass are also analyzed.

2. Experimental

The glasses with the composition of $60TeO_2$–$30WO_3$–$(9.0-x)La_2O_3$–$1.0Tm_2O_3$ –xYb_2O_3 (x = 1.0, 1.5, 2.0, 2.5 in molar ratio) were prepared by the conventional melt-quenching method. The starting materials TeO_2, La_2O_3, Tm_2O_3 and Ho_2O_3 are high purity powder reagents (99.99% minimum), and WO_3 with 99.9% purity. Hereafter, the glasses will be referred as: TWLTm10Yb, TWLTm15Yb, TWLTm20Yb, TWLTm25Yb for x = 1.0, x = 1.5, x = 2.0, x = 2.5, respectively. Another two samples with composition of $60TeO_2$–$30WO_3$–$(10-y)$ La_2O_3–yYb_2O_3 (y = 1.0 and 2.0 in molar ratio) were also prepared for comparison. These glasses are denoted as

* Corresponding author at: Key Laboratory of Materials for High Power Laser, Shanghai Institute of Optics and Fine Mechanics, Chinese Academy of Sciences, P.O. Box 800-211, Shanghai 201800, PR China.
Tel.: +86 21 59914293; fax: +86 21 59914516.
E-mail address: kfli@siom.ac.cn (K. Li).

0925-8388/$ – see front matter © 2010 Elsevier B.V. All rights reserved.
doi:10.1016/j.jallcom.2010.05.162

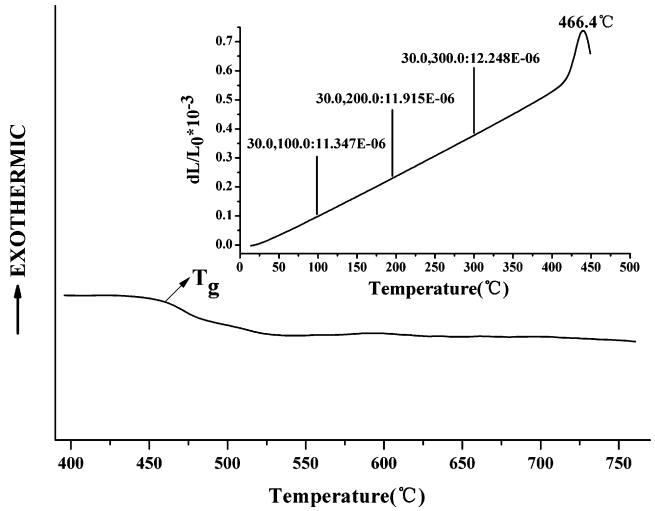

Fig. 1. DTA curve of TWL glass with a heating rate of 10 °C/min. The inset gives the thermal expansion curve of TWL glass.

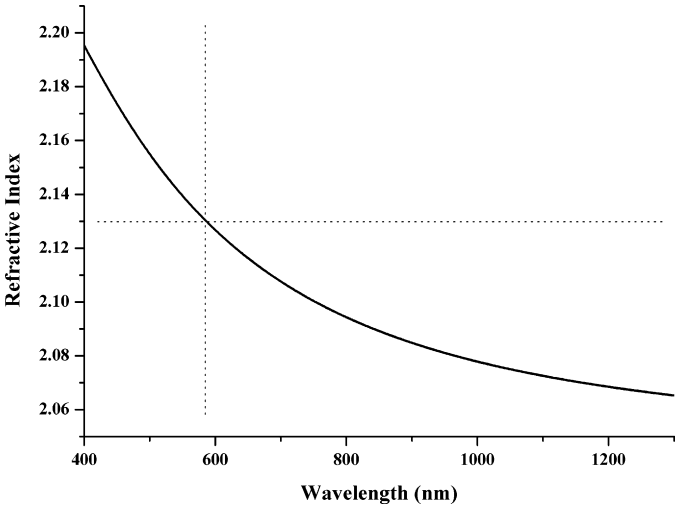

Fig. 2. Refractive index of TWL glass in UV–vis–NIR region.

TWL10Yb and TWL20Yb for $y = 1.0$ and $y = 2.0$, respectively. Batches of approximately 20 g powder were thoroughly mixed and then melted in platinum crucibles at 850–900 °C for 30 min with a closed lid for each batch. The melts were casted at 800 °C into a stainless steel mold and then annealed at 420 °C for 3 h. All the samples were cut and polished to 10 mm × 10 mm × 1 mm for spectroscopic measurements.

The coefficient of thermal expansion was measured using a NETZSCH 402EP with a heating rate of 5 °C/min up to 500 °C. The glass transition temperature (T_g) and onset crystallization temperature (T_x) were analyzed by differential thermal analysis (DTA), using NETZSCH STA 409PC with a heating rate of 10 °C/min. The index of refraction was measured using Metricon Model 2010/M Prism Coupler. The absorption spectra were recorded with a Perkin-Elmer Lambda 900 UV/vis/NIR spectrophotometer in the range of 400–2000 nm. Infrared (IR) transmittance was measured by a thermo nicolet (Nexus FT-IR spectrometer) spectrophotometer. The emission spectra were measured with a Triax 320 type spectrometer (Jobin-Yvon Co., France) excited by 980 nm LD. Lifetimes were measured using FLS920 combined fluorescence lifetime and steady state spectrometer (Edinburgh Instruments). All the measurements were carried out at room temperature.

3. Results and discussion

3.1. Thermal stability, refractive index, infrared transmittance and absorption spectroscopy

Fig. 1 shows the DTA curve of undoped TWL glass and the inset gives the thermal expansion curve of TWL glass. The T_g is 450 °C, and no T_x (onset crystallization temperature) can be observed, which means the sample could be stable against crystallization for fiber drawing. The coefficient of thermal expansion (CTE) is calculated to be 12.248×10^{-6}/°C between 30 and 300 °C, which is much lower than that of ZnO–TeO_2 glass [12]. The relatively low coefficient of thermal expansion is favorable for avoiding thermal damage. The refractive index of TWLTm20Yb glass is collected as a function of wavelength from 400 to 1300 nm as shown in Fig. 2. The refractive index n_d (587.6 nm) of TWLTm20Yb glass is 2.133, which is even higher than that of Bismuthate glass [13]. The high refractive index of the glass is due to the high polarization and molar refraction of TeO_2 and WO_3.

Fig. 3 shows the absorption spectrum of TWLTm20Yb in the range 400–2200 nm and the inset is the IR transmittance spectrum of undoped TWL glass. The IR transmittance reaches 5.2 μm. The absorption spectrum is characterized by transition bands from the $^3H_6$ ground state to the different higher states $^1G_4$, $^3F_{2,3}$, $^3H_4$, $^3H_5$, $^3F_4$ of Tm^{3+}, together with the Yb^{3+} absorption band from the ground state $^2F_{7/2}$ to the excited state $^2F_{5/2}$. Energy levels higher than $^1G_4$ are not observed because of the intrinsic bandgap absorption in the host glass [14]. As expected, all absorption transitions are centered near the wavelengths observed in other matrices for f–f transitions are not easily affected by surrounding ions. The energy level mismatch between Yb^{3+}: $^5F_{5/2}$ and Tm^{3+}: $^3H_5$ is about 1500 cm^{-1}, so energy transfer between Yb^{3+} and Tm^{3+} can be realized by the assistance of one or two phonons. The Oscillator strength (F_{exp}) of the transitions can be calculated using the equation [9]:

$$F_{\exp} = \frac{2.303mc^2}{\pi e^2 N d\lambda^2} \int \mathrm{OD}(\lambda)d\lambda \quad (1)$$

where m is the mass of an electron, e is the charge of an electron, c is the speed of the light in vacuum, N is the concentration of rare earth ions, $\int \mathrm{OD}(\lambda)d\lambda$ is the integrated absorption coefficient, and d is the sample thickness.

According to the Judd–Oflet theory, the theoretical oscillator strength for an electric dipole transition from initial state $|S, L, J\rangle$ to an excited state $|S', L', J'\rangle$ is described by [9,15]:

$$F^{\mathrm{ED}}_{\mathrm{theor}} = \frac{8\pi^2 m\nu}{3h(2J+1)} \left[\frac{(n^2+2)^2}{9n}\right] \sum_{t=2,4,6} \Omega_t \left|\langle S, L, J| \left|U^{\lambda}\right| |S'L'J'\rangle\right|^2 \quad (2)$$

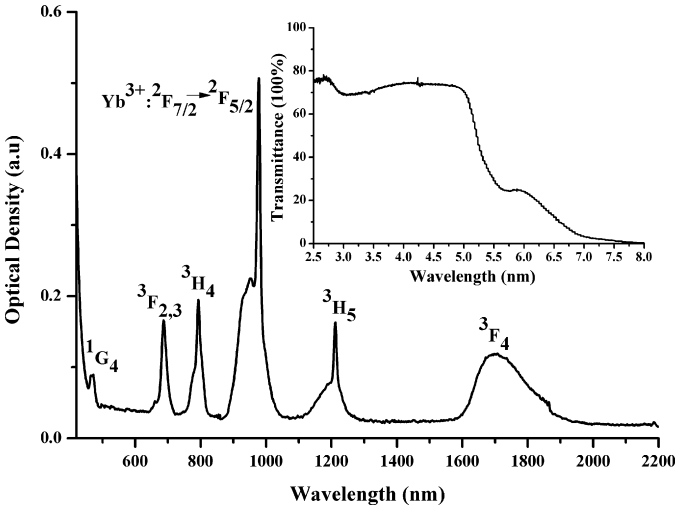

Fig. 3. The absorption spectrum of TWLTm20Yb glass in the range 400–2200 nm. The inset is the IR transmittance spectrum of undoped TWL glass.

Table 1
Measured and calculated values for the oscillator strength in TWLTm20Yb.

Transitions	λ (nm)	Oscillator strength	
		Measured (10^{-6})	Calculated (10^{-6})
$^3H_6 \rightarrow {}^3F_4$	1700	4.420	4.419
$^3H_6 \rightarrow {}^3H_4$	793	4.909	4.908
$^3H_6 \rightarrow {}^3F_{2,3}$	687	4.712	4.710
$^3H_6 \rightarrow {}^1G_4$	464	1.394	1.473

where J is the total angular momentum for the ground state, υ is the transition frequency, $||U^{\lambda}||$ is the reduced matrix element, which is insensitive to the host environment, n is the refractive index, and Ω_t (t = 2, 4, 6) are the J–O intensity parameters. The Ω_t (t = 2, 4, 6) parameters are calculated from the measured values of oscillator strength for different transitions using the least square fitting procedure. The measured absorption oscillator strengths and the values calculated from Eq. (2) are listed in Table 1, the measured and calculated values are consistent well with each other, thus the J–O parameters are reliable. Table 2 shows the J–O parameters of Tm^{3+} in TWL and various other glass matrices. It is well known that Ω_2 is the most sensitive to the covalent bonding [16], so we can reasonable deduce that the covalent degree of the present TWL glass is stronger than that of fluoride and fluorophosphate glasses. On the other hand, the Ω_4/Ω_6 determines the spectroscopy quality of the host materials [19]. Among the glasses listed in Table 2, fluorophosphate glass has the largest Ω_4/Ω_6, and the present TWL glass has a value comparable with Germanate and phosphate glasses. Considering that TWL glass has better stability than fluorophosphate glass, TWL glass is a good matrix for 1.8 μm emission.

The radiative transition probabilities for the excited levels of Tm^{3+} can be calculated using the J–O parameters. The transition probabilities are given by [20]:

$$A[(S,L)J;(S'L')J'] = A_{ed} + A_{md} = \frac{64\pi^4 e^2}{3h\lambda^3(2J+1)}\left[\frac{n(n^2+2)^2}{9}S_{ed} + n^3 S_{md}\right] \quad (3)$$

where $n((n^2+2)^2/9)$ is the local field correction for electric dipole transitions S_{ed} and n^3 for magnetic transitions S_{md}. The S_{md} can be described by [21]:

$$S_{md} = \left(\frac{\hbar}{2mc}\right)^2 \left|\left\langle S,L,J\right|\left|L+2S\right|\left|S'L'J'\right\rangle\right|^2 \quad (4)$$

The $|\langle S,L,J||L+2S||S',L',J'\rangle|^2$ is nonzero only if $\Delta S = \Delta L = 0$, $\Delta J = 0, \pm 1$. The radiative lifetime is related to radiative transitions probabilities by [20]:

$$\tau_{rad} = \left\{\sum_{S',L',J'} A[(S,L)J;(S',L')J']\right\}^{-1} \quad (5)$$

The fluorescence branching ratio can be obtained from the transition probabilities using [20]:

$$\beta_{JJ'} = \beta[(S,L)J;(S',L')J'] = \frac{A[(S,L)J;(S'L')J']}{\sum_{S'L'J'} A[(S,L)J;(S',L')J']} \quad (6)$$

The radiative transition probabilities, banching ratios, and radiative lifetimes of Tm^{3+} in TWL glass are listed in Table 3. The matrix elements are almost host independent, therefore we choose those from Ref. [9]. The radiative transition probability (A_{rad}) of Tm^{3+}: $^3F_4 \rightarrow {}^3H_6$ is 545.8 S^{-1}, which is much higher than that in fluoride, germanate and silicate glasses [22], since the radiative transition probability depends greatly on the refractive index, it is reasonable to obtain large A_{rad} in TWL glass [20,23].

3.2. Fluorescence spectroscopy, cross-sections, and energy transfer processes of Yb^{3+} and Tm^{3+}

The absorption cross-section (σ_{abs}) and stimulated emission cross-section (σ_{em}) are calculated using the Beer–Lambert equation and McCumber theory [24], respectively:

$$\sigma_a(\lambda) = \frac{2.303}{Nl}\mathrm{OD}(\lambda) \quad (7)$$

$$\sigma_e(\lambda) = \sigma_a(\lambda)\frac{Z_l}{Z_u}\exp\left(\frac{E_{zl} - hc\lambda^{-1}}{kT}\right) \quad (8)$$

where $\mathrm{OD}(\lambda)$ is the optical density of Tm^{3+} or Yb^{3+} at wavelength λ, N is the concentration (ions/cm^3) of the dopants, l is the sample thickness. Z_u and Z_l denote the partition functions of upper and lower states, respectively. The term E_{zl}, the so-called "zero-line" energy, is defined as the energy separation between the lowest crystal field levels of the upper and lower manifolds. The ratio Z_l/Z_u is 1.3 for Yb^{3+} [9]. Fig. 4 shows the cross-sections of Tm^{3+}:$^3H_6$–$^3H_5$ and Yb^{3+}:$^5F_{7/2}$–$^5F_{5/2}$, respectively. We can see the absorption cross-section of Yb^{3+} is much larger than that of Tm^{3+}. The inset shows

Table 2
The Judd–Ofelt parameters of Tm^{3+} in TWL and various other glass matrices.

Glasses	Ω_2 (10^{-20} cm^2)	Ω_4 (10^{-20} cm^2)	Ω_6 (10^{-20} cm^2)	Ω_4/Ω_6	Reference
ZBLAN	1.96	1.36	1.16	1.17	[9]
Silica	6.23	1.91	1.36	1.40	[9]
Germanate	5.55	2.03	1.26	1.61	[17]
Phosphate	5.63	1.75	1.11	1.58	[18]
Fluorophosphate	4.12	1.47	0.72	2.04	[9]
TWL	4.48	1.87	1.30	1.44	This work

Table 3
Calculated radiative rates, lifetimes, and branching ratios of Tm^{3+} in TWL glass.

Transition	$\lvert U^{(2)}\rvert^2$	$\lvert U^{(4)}\rvert^2$	$\lvert U^{(6)}\rvert^2$	λ (nm)	A_{ed} (S^{-1})	A_{md} (S^{-1})	β	τ_R (μs)
$^3F_4 \rightarrow {}^3H_6$	0.5374	0.7261	0.2382	1785	545.8		1	1832
$^3H_5 \rightarrow {}^3H_6$	0.1074	0.2314	0.6383	1200	650.9	130.6	0.977	1279
$^3F_4$	0.0913	0.1280	0.9276	4315	21.5		0.023	
$^3H_4 \rightarrow {}^3H_6$	0.2372	0.1090	0.5947	788	3278.9		0.907	275
$^3F_4$	0.1292	0.1301	0.2055	1490	57.7	23.1	0.066	
$^3H_5$	0.0131	0.4786	0.0093	2290	283.2		0.027	
$^3F_{2,3} \rightarrow {}^3H_6$	0.0000	0.3164	0.8497	685	5419.6		0.825	152
$^3F_4$	0.0025	0.0005	0.1670	1130	176.9	154.3	0.051	
$^3H_5$	0.6286	0.3458	0.0000	1550	806.5		0.123	
$^3H_4$	0.0821	0.3536	0.2850	5552	9.0		0.001	

Table 4
Energy transfer parameters of Yb^{3+} and Tm^{3+} in TWLTm20Yb glass.

	N (number of phonons) (% phonon assisted)			C_{D-A} (10^{-40} cm^6/s)	C_{D-D}(10^{-40} cm^6/s)	R_c (nm)
$Yb^{3+} \rightarrow Tm^{3+}$	0	1	2	3.67	...	0.83
	0	46.7	53.3			
$Yb^{3+} \rightarrow Yb^{3+}$	0		1	...	67.30	1.15
	98.2		1.8			

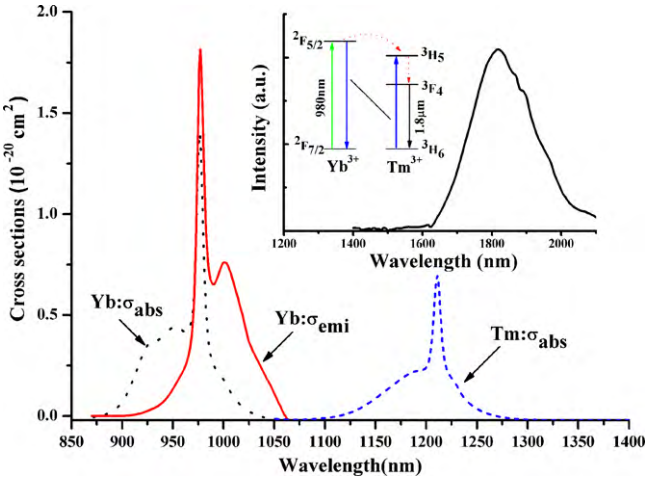

Fig. 4. Absorption (dash line) and emission cross-section (solid line) corresponding to $^2F_{7/2}$–$^2F_{5/2}$ of Yb^{3+} and $^3H_6$–$^3H_5$ of Tm^{3+} in TWL glass. The inset is the emission spectrum of Tm^{3+} in TWLTm20Yb under the excitation of 980 nm LD and the energy transfer mechanism from Yb^{3+} to Tm^{3+}.

the intense emission at 1.8 μm assigned to $^3F_4 \rightarrow {}^3H_6$ transition of Tm^{3+}. In order to provide better understanding of the energy transfer process, the energy transfer mechanism in TWLTm20Yb is also illustrated in the inset. One Yb^{3+} ion absorbs the 980 nm photon and is excited to the $^2F_{5/2}$ energy level. Then the excited Yb^{3+} transfers its energy to the Tm^{3+} via (Yb^{3+}:$^2F_{5/2}$,Tm^{3+}:$^3H_6$) → (Yb^{3+}:$^2F_{7/2}$, Tm^{3+}:$^3H_5$), which is assisted by one or more phonons. The Tm^{3+} ion at $^3H_5$ state relaxes to $^3F_4$ state quickly and emits a photon via $^3F_4 \rightarrow {}^3H_6$ transition. The probability rate of energy transfer between Yb^{3+} and Tm^{3+} can be estimated as [9,25,26]:

$$W_{D-A} = \left(\frac{2\pi}{\hbar}\right) \left|H_{DA}\right|^2 S_{DA}^N \tag{9}$$

where $|H_{DA}|$ is the matrix element of the perturbation Hamiltonian between initial and final states in the energy transfer process, S_{DA}^N is the integral overlap between the m-phonon emission sideband of donor ions (D, here D stands for Yb^{3+}) and k-phonon absorption line shapes of acceptor ions (A, here A stands for Tm^{3+}) and N is the total phonons in the transfer process ($m+k=N$) [25]. In the case of weak electron–phonon coupling which is suitable for RE ions, S_{DA}^N can be approximated by [26]:

$$S_{DA}^N \approx \sum e^{-\left(S_0^D+S_0^A\right)} \left[\frac{\left(S_0^D+S_0^A\right)^N}{N!}\right] S_{DA}(0,0,E)\,\delta\left(N, \frac{\Delta E}{\hbar w_0}\right) \tag{10}$$

where S_0^D and S_0^A are the Huang–Rhys factors of the Yb^{3+} and Tm^{3+} in TWL glass. $S_{DA}(0, 0, E)$ represents the overlap between the zero phonon emission line shape of Yb^{3+} and zero phonon absorption line shape of Tm^{3+} ions. $S_{DA}(0, 0, E) \approx 0$ in the case of nonresonant energy transfer, unless one takes the zero-phonon line shape of Yb^{3+} emission as $g_{emi}^D(E - \Delta E)$ with ΔE = energy mismatch. Then the integral overlap in the case of m-phonon emission can be expressed as [9]:

$$S_{DA}(m,0,E) = \int g_{emis(m\text{-phonon})}^D(E) g_{abs}^A(E) dE = \frac{S_0^m}{m!} e^{-S_0} S_{DA}(0,0,E)$$
$$= \int \left[\frac{S_0^m}{m!} e^{-S_0} \int g_{emis}^D(E-\Delta E)\right] g_{abs}^A(E) dE \tag{11}$$

where $\Delta E = m\hbar\omega_0$. For the measurements carried out at some finite temperature T, the multi-phonon probability must be included, then the emission cross-section (σ_{em}) of Yb^{3+} with m phonon emission and absorption cross-section (σ_{abs}) of Tm^{3+} with k-phonon absorption can be proposed as [26]:

$$\sigma_{emis(m\text{-phonon})}^D = \sigma_{emis}^D\left(\lambda_m^+\right) \approx \frac{S_0^m e^{-S_0}}{m!} (\bar{n}+1)^m \sigma_{emis}^D(E-E_1) \tag{12}$$

$$\sigma_{abs(k\text{-phonon})}^A = \sigma_{abs}^A\left(\lambda_k^-\right) \approx \frac{S_0^k e^{-S_0}}{k!} (\bar{n})^k \sigma_{abs}^A(E+E_2) \tag{13}$$

where $\lambda_m^+[= 1/(1/\lambda - m\hbar\omega_0)]$ and $\lambda_k^-[= 1/(1/\lambda + k\hbar\omega_0)]$ are the wavelengths of Yb^{3+} with m phonon creation and Tm^{3+} with k-phonon annihilation, respectively. $E_1 = m\hbar\omega_0$, $E_2 = k\hbar\omega_0$, and $\Delta E = E_1 + E_2$. If we ignore the k-phonon annihilation process and just focus on the m phonon creation process, the probability rate of energy transfer can be obtained using the following direct transfer equation [9,26]:

$$W_{DA}(R) = \frac{6cg_{low}^D}{(2\pi)^4 n^2 R^6 g_{up}^D} \sum_{m=0}^{\infty} e^{-(2\bar{n}+1)S_0} \frac{S_0^m}{m!} (\bar{n}+1)^m$$
$$\times \int \sigma_{emis}^D\left(\lambda_m^+\right) \sigma_{abs}^A(\lambda)\, d\lambda = \frac{C_{DA}}{R^6} \tag{14}$$

where R is the distance of separation between donor and acceptor, C_{D-A} is the energy transfer coefficient (cm^6/s), and $\bar{n} = 1/(e^{\hbar\omega_0/kT} - 1)$ is the average occupancy of phonon modes at temperature T. The energy transfer coefficient is then expressed by:

$$C_{DA} = \frac{6cg_{low}^D}{(2\pi)^4 n^2 g_{up}^D} \sum_{m=0}^{\infty} e^{-(2\bar{n}+1)S_0} \frac{S_0^m}{m!} (\bar{n}+1)^m \int \sigma_{emis}^D\left(\lambda_m^+\right) \sigma_{abs}^A(\lambda) d\lambda. \tag{15}$$

The critical radius of the interaction can be obtained using [26]:

$$R_C^6 = C_{D-A}\tau_D \tag{16}$$

TWLTm20Yb shows the most intense emission among the samples. The energy transfer properties of Yb^{3+} and Tm^{3+} in this sample are listed in Table 4. The energy transfer from Yb^{3+} to Tm^{3+} is assisted by one (46.7%) and two (53.3%) phonons because of the very little overlap between the Yb^{3+} emission cross-section and the Tm^{3+} absorption cross-section as shown in Fig. 4. It is found that the energy transfer coefficient in TWLTm20Yb glass is 3.67×10^{-40} cm^6/s, which is larger than in fluoride crystals and glasses [27,28].

In the Tm^{3+}/Yb^{3+} codoped TWL glasses, the energy transfer efficiency η from Yb^{3+} to Tm^{3+} can be expressed as [9]:

$$\eta = 1 - \frac{\tau_{Yb}}{\tau_{Yb}^0} \tag{17}$$

where τ_{Yb} and τ_{Yb}^0 are the lifetimes of Yb^{3+} with and without Tm^{3+} codoping. The decay curves in samples are plotted in Fig. 5. It can

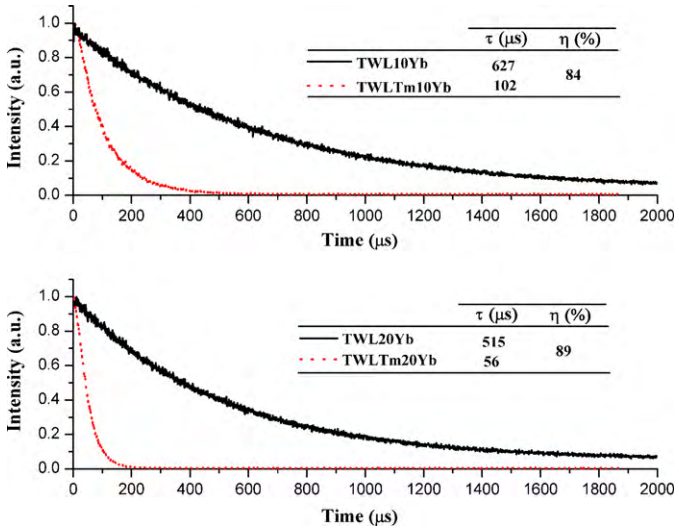

Fig. 5. The decay curves (solid and dash lines) of the glasses obtained under the excitation of 980 nm laser diode.

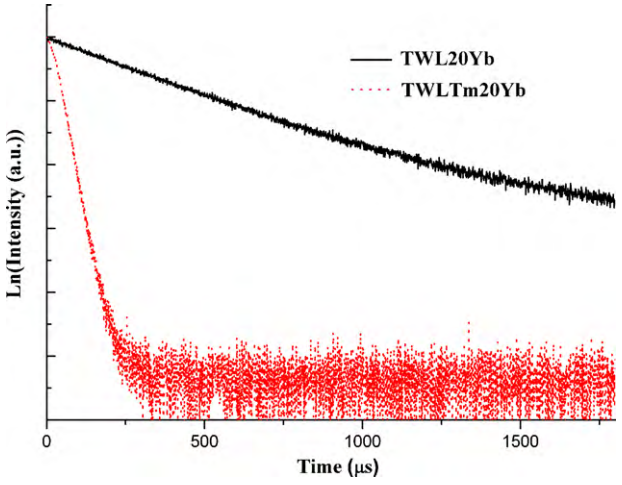

Fig. 6. The semi-log plot of intensity vs decay time.

be seen that the lifetime of Yb^{3+} reduces greatly by codoping with Tm^{3+}, which means efficient energy transfer from Yb^{3+} to Tm^{3+}. In TWLTm20Yb glass, the energy transfer efficiency from Yb^{3+} to Tm^{3+} is 89%, which is much higher than that reported in Ref. [29], and is also higher than that in germanate glasses [9]. Fig. 6 shows the Ln(Intensity (a.u.)) versus lifetime of Yb^{3+} in TWL20Yb and TWLTm20Yb glasses. It can be found that the decay curve of Yb^{3+} in TWL20Yb is approximately single-exponential. Codoping TWL20Yb with Tm^{3+} produces a decay curve that is not described by a single-exponential, indicating efficient energy transfer from the Yb^{3+} to Tm^{3+} ions.

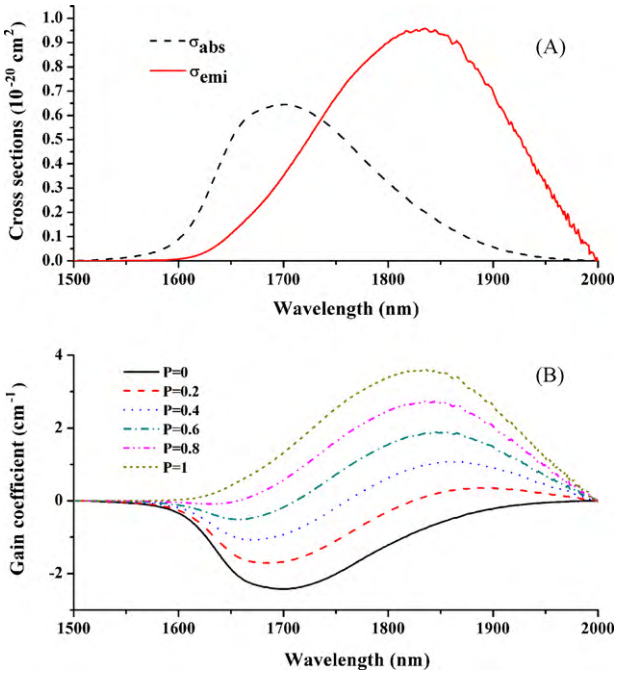

Fig. 7. Absorption, emission cross-sections (A) and gain coefficient (B) corresponding to $^3F_4 \rightarrow {}^3H_6$ transition of Tm^{3+} in TWL glass.

3.3. Cross-sections and gain coefficient of Tm^{3+} at 1.8 μm

Fig. 7(A) shows the absorption cross-section (σ_{abs}) and emission cross-section (σ_{em}) corresponding to $^3F_4 \leftrightarrow {}^3H_6$ transitions of Tm^{3+}, which are calculated using Eqs. (7) and (8). The maximum emission cross-sections of Tm^{3+} in TWL glass and other common glasses are listed in Table 5. It is found that the peak of the σ_{em} in TWL glass is larger than that in Fluorophosphate [13], Bismuthate [13], Germanate [17] and Fluoride [30] glasses. The large σ_{em} is mainly due to the high refractive index of the glass host and the high spontaneous transition probability, which can be favorable for achieving intense 1.8 μm emission. The product of emission cross-section and lifetime ($\sigma_{em}\tau_R$) is of significance in achieving high gain [8]. The values of $\sigma_{em}\tau_R$ are listed in Table 5. The value of $\sigma_{em}\tau_R$ in TWL glass is smaller than that in fluoride glass [30], but larger than that in Germanate [17], Bismuthate [13], and Fluorophosphate [13] glasses. The large value of $\sigma_{em}\tau_R$ indicates that high gain could be achieved in TWL glass. The room temperature gain coefficient can be simply evaluated by [8]:

$$G(\lambda, P) = N[P\sigma_{em}(\lambda) - (1-P)\sigma_{abs}(\lambda)] \quad (18)$$

where $N = 3.76 \times 10^{20}$ ions/cm^3 is the total concentration of Tm^{3+} and P is the population inversion given by the ratio between the population of Tm^{3+}:$^3F_4$ level and the total Tm^{3+} concentration. The calculated gain coefficient versus wavelength for different population inversion parameters P is shown in Fig. 7(B). The maximum gain coefficient at around 1835 nm is 3.6 cm^{-1}, which is about two times greater than the value reported in Ref. [31]. It is noted that the gain coefficient increases and the gain band extends to longer

Table 5
Calculated emission cross-section σ_{em}, radiative lifetime τ_R, and $\sigma_{em} \times \tau_R$ corresponding to $^3F_4 \rightarrow {}^3H_6$ transition of Tm^{3+} in TWL and various other glasses.

Glasses	σ_{em} ($\times 10^{-21}$ cm^2)	τ_R (ms)	$\sigma_{em} \times \tau_R$ ($\times 10^{-21}$ cm^2 ms)	Reference
Fluorophosphate	2.50	1.80	4.50	[13]
Bismuthate	6.70	2.60	17.40	[13]
Germanate	7.70	1.77	13.63	[17]
Fluoride	2.31	11.10	25.64	[30]
TWL	9.60	1.83	17.56	This work

wavelength with increasing values of *P*, which indicates that the potential lasing wavelength varies as the pump power is increased [32].

4. Conclusions

In conclusion, the thermal stability, absorption, IR transmittance and infrared fluorescence of Tm^{3+}/Yb^{3+} codoped TWL glasses were investigated. Intense 1.8 μm emission was obtained under the excitation of 980 nm laser diode. The spectroscopic properties of Tm^{3+} doped TWL glass were analyzed by calculating the *J–O* parameters, the radiative transition rates, and the branching ratios. The peak emission cross-section of Tm^{3+}:$^3F_4 \rightarrow {}^3H_6$ transition was calculated to be 9.6×10^{-21} cm^2 and the high gain around 1.8 μm was predicted by the large $\sigma_{em}\tau_R$ product (17.56×10^{-21} cm^2 ms). Large energy transfer coefficient (3.76×10^{-40}cm^6/s) and high energy transfer efficiency (89%) from Yb^{3+} to Tm^{3+} can be obtained by the assistance of one or two phonons. The maximum gain coefficient at around 1835 nm is 3.6 cm^{-1}. The present results indicate that TWL glass is a promising host material for a 1.8-μm laser.

Acknowledgements

This research was financially supported by the Chinese National Natural Science Foundation (grant 60607014 and grant 50672107) and the Chinese National 863 Project (No. 2007AA03Z441). The authors appreciate Dr. Tyler Mullenbach for his help in paper preparation.

References

[1] B. Richards, A. Jha, Y. Tsang, D. Binks, J. Lousteau, F. Fusari, A. Lagatsky, C. Brown, W. Sibbett, Laser Phys. Lett. 7 (2010) 177.
[2] D. Zhou, Z. Song, G. Chi, J. Qiu, J. Alloys Compd. 481 (2009) 881.
[3] S.F. León-Luis, J. Abreu-Afonso, J. Peña-Martínez, J. Méndez-Ramos, A.C. Yanes, J. del-Castillo, V.D. Rodríguez, J. Alloys Compd. 479 (2009) 557.
[4] J. Ding, Q. Zhang, J. Cheng, X. Liu, G. Lin, J. Qiu, D. Chen, J. Alloys Compd. 495 (2010) 205.
[5] Q. Zhang, G. Chen, G. Zhang, J. Qiu, D. Chen, J. Appl. Phys. 106 (2009) 113102.
[6] M. Liao, L. Wen, H. Zhao, Y. Fang, H. Sun, L. Hu, Mater. Lett. 61 (2007) 470.
[7] Y. Jeong, P. Dupriez, J.K. Sahu, J. Nilsson, D.Y. Shen, W.A. Clarkson, S.D. Jackson, Electron. Lett. 41 (2005) 173.
[8] B. Zhou, E.Y. Pun, H. Lin, D. Yang, L. Huang, J. Appl. Phys. 106 (2009) 103105.
[9] Q. Zhang, G. Chen, G. Zhang, J. Qiu, D. Chen, J. Appl. Phys. 107 (2010) 023102.
[10] M. Liao, Y. Fang, H. Sun, L. Hu, Opt. Mater. 29 (2007) 867.
[11] K. Li, G. Wang, L. Hu, J. Zhang, J. Hu, J. Inorg. Mater. 25 (2010) 429.
[12] F.E.P. dos Santos, F.C. Fávero, A.S.L. Gomes, J. Xing, Q. Chen, M. Fokine, I.C.S. Carvalho, J. Appl. Phys. 105 (2009) 4512–4521.
[13] H. Fan, G. Gao, G. Wang, J. Hu, L. Hu, Opt. Mater. 32 (2010) 627.
[14] R. Balda, J. Fernández, S.G. Revilla1, J.M. Navarro, Opt. Express 15 (2007) 6750.
[15] M. Shojiya, Y. Kawamoto, K. Kadono, J. Appl. Phys. 89 (2001) 4944.
[16] C.K. Jorgensen, R. Reisfeld, J. Less-Common Met. 93 (1983) 107.
[17] R. Balda, L.M. Lacha, J. Fernandez, J.M. Fernandez-Navarro, Opt. Mater. 27 (2005) 1771.
[18] A. Kermaoui, F. Pellïe, J. Alloys Compd. 469 (2009) 601.
[19] P.R. Watekar, S. Ju, W.T. Han, J. Non-Cryst. Solids 354 (2008) 1453.
[20] R. Balda, L.M. Lacha, J. Fernández, M.A. Arriandiaga, J.M.F. Navarro, D.M. Martin, Opt. Express 16 (2008) 11836.
[21] B.M. Walsh, N.P. Barnes, B. Di Bartolo, J. Appl. Phys. 83 (1998) 2772.
[22] B. Peng, T. Izumitani, Opt. Mater. 4 (1995) 797.
[23] G. Gao, L. Hu, H. Fan, G. Wang, K. Li, S. Feng, S. Fan, H. Chen, J. Pan, J. Zhang, Opt. Mater. 32 (2009) 402.
[24] D.E. McCumber, Phys. Rev. 136 (1964) 954.
[25] T. Miyakawa, D.L. Dexter, Phys. Rev. B 1 (1970) 2961.
[26] L.V.G. Tarelho, L. Gomes, I.M. Ranieri, Phys. Rev. B 56 (1997) 14344.
[27] Y. Mita, T. Ide, M. Togashi, H. Yamamoto, J. Appl. Phys. 85 (1999) 4160.
[28] Y. Mita, H. Kawashima, N. Sawanobori, Jpn. J. Appl. Phys. Part 2 38 (1999) L746.
[29] Y. Tsang, B. Richards, D. Binks, J. Lousteau, A. Jha, Opt. Express 16 (2008) 10690.
[30] B.M. Walsh, N.P. Barnes, Appl. Phys. B Lasers Opt. 78 (2004) 325.
[31] S. Yu, Z. Yang, S. Xu, Opt. Mater. 31 (2009) 1723.
[32] X.L. Zou, H. Toratani, J. Non-Cryst. Solids 195 (1996) 113.